Subunit stoichiometry and arrangement in a heteromeric glutamate-gated chloride channel

Nurit Degani-Katzav, Revital Gortler, Lilach Gorodetzki, and Yoav Paas[1]

Laboratory of Ion Channels, The Mina and Everard Goodman Faculty of Life Sciences and The Institute of Nanotechnology and Advanced Materials, Bar-Ilan University, Ramat Gan 52900, Israel

Edited by Arthur Karlin, Columbia University, College of Physicians and Surgeons, New York, NY, and approved December 2, 2015 (received for review December 16, 2014)

The invertebrate glutamate-gated chloride-selective receptors (GluClRs) are ion channels serving as targets for ivermectin (IVM), a broad-spectrum anthelmintic drug used to treat human parasitic diseases like river blindness and lymphatic filariasis. The native GluClR is a heteropentamer consisting of α and β subunit types, with yet unknown subunit stoichiometry and arrangement. Based on the recent crystal structure of a homomeric GluClαR, we introduced mutations at the intersubunit interfaces where Glu (the neurotransmitter) binds. By electrophysiological characterization of these mutants, we found heteromeric assemblies with two equivalent Glu-binding sites at β/α intersubunit interfaces, where the GluClβ and GluClα subunits, respectively, contribute the "principal" and "complementary" components of the putative Glu-binding pockets. We identified a mutation in the IVM-binding site (far away from the Glu-binding sites), which significantly increased the sensitivity of the heteromeric mutant receptor to both Glu and IVM, and improved the receptor subunits' cooperativity. We further characterized this heteromeric GluClR mutant as a receptor having a third Glu-binding site at an α/α intersubunit interface. Altogether, our data unveil heteromeric GluClR assemblies having three α and two β subunits arranged in a counterclockwise β-α-β-α-α fashion, as viewed from the extracellular side, with either two or three Glu-binding site interfaces.

allostery | Cys-loop receptors | ion channels | ivermectin | neurotransmitters

Glutamate-gated chloride-selective receptors (GluClRs) are pentameric glutamate-gated chloride channels unique to invertebrates. They belong to the Cys-loop receptor superfamily of transmembrane oligomers that open an intrinsic cationic or anionic channel pore upon binding of neurotransmitters, such as ACh, serotonin, GABA, Gly, histamine, or Glu (1–9). GluClRs are specific targets for ivermectin (IVM), a broad-spectrum anthelmintic drug used to treat filarial diseases like onchocerciasis (river blindness) and elephantiasis (lymphatic filariasis) that afflict hundreds of millions of people worldwide (10, 11). IVM is also broadly used in cattle, swine, and pets to kill gastrointestinal roundworms, lungworms, grubs, sucking lice, and mange mites (12). The high efficiency of IVM stems from its capacity to act as an agonist that keeps the receptor's ion channel continuously open (13–18). Because the GluClR is chloride-selective, IVM causes sustained hyperpolarization across postsynaptic membranes in the parasitic nematodes. This long-term hyperpolarization leads to suppression of excitation in motor neurons and inhibition of locomotion (19); inhibition of the pharyngeal muscle activity, which interrupts with feeding behavior (20); and interruption of secretion processes that are crucial for evading the host immune system (21).

Genes encoding two GluClR homologous subunits, GluClα and GluClβ (*glc-1* and *glc-2*, respectively), were first cloned from *Caenorhabditis elegans* (13). When expressed in *Xenopus* oocytes, homomeric GluClαRs respond to IVM but not to Glu and, in contrast, homomeric GluClβRs respond to Glu but not to IVM (13, 16, 17, 22). A recent 3D crystal structure of a truncated homomeric GluClαR ($GluCl\alpha_{cryst}R$; Protein Data Bank ID code 3RIF) shows that when IVM is bound at the five α/α intersubunit interfaces in the ion-channel pore periphery, Glu is lodged at the five α/α intersubunit interfaces in the ligand-binding domain (LigBD) (23) (Fig. 1*A*). These Glu-binding sites are homologous to the neurotransmitter/agonist-binding sites of other Cys-loop receptors (1, 2, 24), bacterial homologs of Cys-loop receptors (25–30), and ACh-binding proteins (31–34).

Importantly, the naturally occurring GluClR robustly responds to both Glu and IVM independently; therefore, it is considered to consist of both GluClα and GluClβ subunit types (13–18). However, little is known about the stoichiometry and molecular arrangement of the subunits in heteromeric GluClRs. Furthermore, the aforementioned crystallographic observations (23) are consistent with earlier studies showing that Glu elicits current responses in homomeric GluClαRs only when applied after activation by IVM (14), which gives rise to the following question: Could an α/α intersubunit interface be formed in a heteromeric assembly, bind Glu, and functionally participate in the activation process even without IVM preassociation? To resolve this question, we clarified here the stoichiometry and positions of the α and β subunits in GluClα/βR heteromeric assemblies that carry mutations in both the putative Glu- and IVM-binding pockets.

Results

Can the Coupling Loops of the GluClα Subunit Mediate Channel Opening upon Glu Binding? Based on the capability of the WT homomeric GluClα (GluClαWT) receptor to respond to Glu only following exposure to IVM, it was suggested that IVM binding induces a conformational change that enables coupling of Glu binding at α/α intersubunit interfaces to the opening of the ion-channel gate (14, 23). To explore this suggestion further, we used a strategy of microchimerism that is based on previous studies showing that in various Cys-loop receptors, the β1β2, Cys, and β8β9 loops of the

Significance

Cys-loop receptors (CLRs) are transmembrane ion channels activated by neurotransmitters to mediate chemoelectric excitation or inhibition throughout the nervous system. Hence, CLRs play a key role in our day-to-day life, from coordination of motions to cognition. Impairment of CLRs' activity leads to various pathophysiological conditions. The CLR studied here is a glutamate-gated chloride-selective receptor (GluClR). GluClRs are unique to invertebrates, yet they are pharmacologically important because they serve as targets for ivermectin, an anthelmintic drug used to treat humans suffering from filarial diseases. This study provides better understanding of the subunit arrangement and stoichiometry of Glu-binding sites in GluClRs.

Author contributions: N.D.-K. and Y.P. designed research; N.D.-K., R.G., L.G., and Y.P. performed research; N.D.-K., R.G., L.G., and Y.P. analyzed data; and N.D.-K. and Y.P. wrote the paper.

The authors declare no conflict of interest.

This article is a PNAS Direct Submission.

[1]To whom correspondence should be addressed. Email: yoav.paas@biu.ac.il.

This article contains supporting information online at www.pnas.org/lookup/suppl/doi:10.1073/pnas.1423753113/-/DCSupplemental.

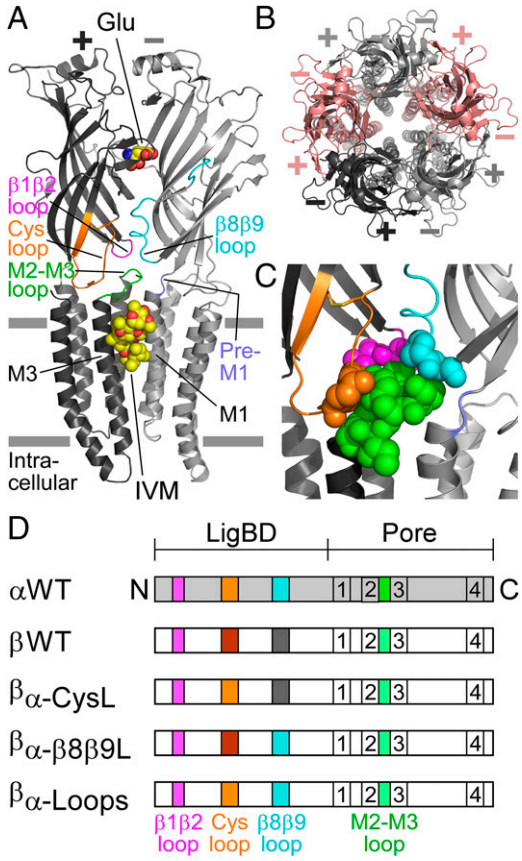

Fig. 1. Structural characteristics of GluClRs. (*A*) Two neighboring subunits of the homopentameric GluClα_{cryst}R [Protein Data Bank (PDB) ID code 3RIF] are shown from the side in light and dark gray colors. Wide gray horizontal lines mark the putative membrane borders. The four coupling loops are colored as shown in *C* and the upper row of *D*. Glu and IVM are shown as space-filling models with carbon, oxygen, and nitrogen atoms colored in yellow, red, and blue, respectively. They are bound at the α(+)/α(–) intersubunit interface far away from each other: Glu in the extracellular LigBD and IVM in the upper part of the pore-domain periphery, between M1 (of the light gray subunit) and M3 (of the dark gray subunit). Note that in Cys-loop receptors, the principal and complementary faces of a neurotransmitter-binding pocket are formed by the (+) and (–) sides of two adjacent subunits, respectively. (*B*) Top view of the GluClα_{cryst} pentamer showing five identical subunits, which are colored differently to highlight the intersubunit interfaces located between the (+) and (–) sides. (*C*) Space-filling models of residues belonging to the coupling loops, which create an extensive bond network at the interface between the LigBD and the ion-channel pore domain. (*D*) Schemes of GluClR subunits used in this study. The M1–M4 transmembrane segments are numbered 1–4. Different colors reflect differences in amino acid sequences (Fig. S1).

LigBD interact with the M2–M3 loop of the pore domain to couple neurotransmitter binding to channel gating (23, 35–44) (e.g., Fig. 1 *A* and *C*). These four loops are termed the coupling loops. Fig. 1*D* shows schemes of the WT GluClα and GluClβ subunits, as well as three microchimeric GluClβ subunits where we replaced the Cys loop, β8β9 loop, or both loops with the homologous loops of the GluClα subunit. These microchimeric subunits are termed GluCl$\beta_{\alpha\text{-CysL}}$, GluCl$\beta_{\alpha\text{-}\beta8\beta9L}$, and GluCl$\beta_{\alpha\text{-Loops}}$, respectively. Note that the *C. elegans* GluClα and GluClβ subunits share an identical β1β2 loop sequence, whereas their M2–M3 loop sequence is almost identical (Fig. S1).

CHO cells transfected with the GluClαWT subunit alone showed very weak responses to 10 mM Glu (135 ± 27 pA in eight cells; mean ± SEM), but responded well to 500 nM IVM (Fig. S2*B*; 14 cells). This observation is in line with the findings of Frazier et al. (45), who reported that HEK cells expressing GluClα homomers are responsive to IVM but not to Glu. CHO cells transfected with the GluClβWT subunit alone showed very weak, rare responses to 10 mM Glu (less than 230 pA in eight cells; Fig. S2*A*), in line with results obtained in HEK cells (45). No responses to 500 nM IVM in CHO cells transfected with the GluClβWT subunit alone were observed (10 cells), in agreement with the same observations in HEK cells (18, 22). In contrast to these differential responses, cells cotransfected with both GluClαWT and GluClβWT subunits displayed robust responses to 1.5 mM Glu (EC_{50} concentration) and 500 nM IVM (Fig. S2*C*). We therefore deduce that robust responses to Glu and IVM (independently) in a cell cotransfected with the GluClαWT and microchimeric GluClβ subunits (Fig. S2 *D–F*) reflect the function of heteromeric GluClα/βR complexes. This deduction also applies for the site-specific mutants discussed further below.

Fig. 2 shows representative current traces elicited by increasing Glu concentrations (Fig. 2*A*) and the corresponding dose–response curves (Fig. 2*B*) for the heteromeric WT and microchimeric GluClRs. The Glu-EC_{50} values specified in Table S1 indicate that the apparent affinities of the GluClαWT/$\beta_{microchimeric}$ receptors for Glu were very close to the apparent affinity of the GluClαWT/βWT receptor. The Hill coefficients of all four receptors (Table S1) were >1, indicating their activation with positive cooperativity. Note that the Glu-EC_{50} and the Hill coefficient determined here for the GluClαWT/βWT receptor (Table S1) are very close to those values determined in *Xenopus* oocytes [Glu-EC_{50} = 1.36 ± 0.05 mM and Hill coefficient (n_H) = 1.7 ± 0.1] (13). Remarkably, Glu readily activates the GluClαWT/$\beta_{\alpha\text{-Loops}}$ receptor, all of whose LigBD's coupling loops are of the GluClα subunit (Fig. 2 and Table S1). We thus conclude that the β1β2, Cys, and β8β9 loops of the GluClα subunit are inherently capable of coupling Glu binding to pore gating, with no need for IVM prebinding.

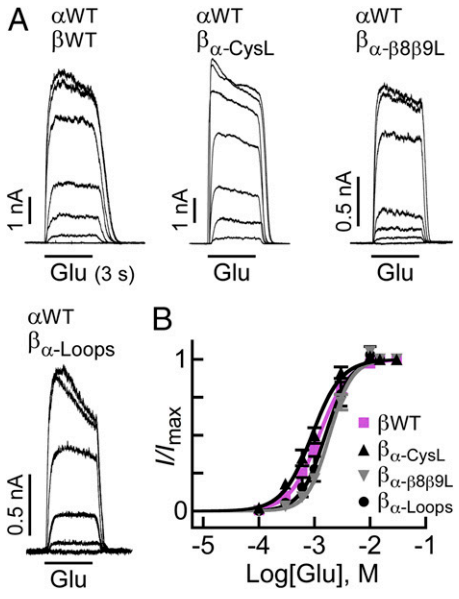

Fig. 2. Glu-activation properties of WT and microchimeric GluClRs. (*A*) Representative Glu-elicited currents measured in cells cotransfected with the indicated subunits. In all cases, Glu was applied for 3 s. Glu concentrations: 0.1 mM, 0.3 mM, 0.6 mM, 1 mM, 3 mM, 10 mM, and 30 mM in the upper row and 0.1 mM, 0.3 mM, 0.6 mM, 1 mM, 10 mM, and 30 mM in the lower row. Measurements were performed at +60 mV. (*B*) Dose–response curves plotted for responses measured in cells cotransfected with the GluClαWT subunit and the GluClβ subunits indicated in the figure. Curves were fitted to the averaged data points with a nonlinear regression using the Hill equation (Eq. **1**) ($r^2 > 0.99$). Error bars correspond to SEM.

Contribution of the GluClα Subunit (−) Side to Glu Accommodation in Heteromeric GluClR Mutants. The aforementioned observations brought us to the recognition that a thorough study of how the GluClα subunit contributes to Glu binding in heteromeric GluClRs is necessary. Therefore, we first introduced mutations in the (−) side of the GluClα subunit based on the crystal structure of the homomeric $GluCl\alpha_{cryst}R$ (23) [the (−) and (+) subunit sides are defined in Fig. 1 *A* and *B*]. This structure indicates that the δ-guanidino groups of α(−)R98 and α(−)R117 are at an appropriate distance to form ion pairing with the α- and γ-carboxyl groups of Glu, respectively (Fig. 3*D*). A mutation that eliminated the charge and drastically reduced the side-chain size of α(−)R117, but kept hydrophilicity at this position (i.e., R→S), did not provide a functional GluClαR117S/βWT receptor. We therefore replaced the two Args (one at a time) with a more conservative and bulkier hydrophilic residue, Asn or Gln, which can function as hydrogen bond donor (or acceptor) with no capability to form salt bridges. A mutant having an αR98N substitution (GluClαR98N/βWT receptor) provided robust responses, but very high Glu concentrations were necessary to reach saturation [Fig. 3*A*, traces (*Right*) and brownish dose–response curve (*Left*)]. Note that to dissolve Glu, it was titrated with equimolar concentrations of NaOH; therefore, we did not change the Nernst potential for Cl^- during Glu application. However, the osmolarity and negative charge of the external solution drastically increased during the application of high Glu concentrations (for 0.6 s). Even so, we assume that these factors did not affect the responses, as discussed in *SI Text*, section 1, in conjunction with Fig. S3.

In the case of the GluClαR117N/βWT receptor, the current responses did not allow us to analyze the dose–response relation reliably because they were very low (~300 pA at 1 M Glu) and did not reach saturation, unlike in the case of the GluClαR98N/βWT receptor. In contrast, introducing Q at position α(−)117, which has a longer side chain than N, created a responsive GluClαR117Q/βWT receptor that enabled us to determine its Glu-EC_{50} and Hill coefficient (Fig. 3*A* and Table S1).

The crystal structure also indicates that α(−)S182 forms a hydrogen bond with the γ-carboxyl group of Glu (23) (Fig. 3*D*). Preventing this hydrogen bonding in the heteromeric GluClαS182A/βWT receptor produced an effect similar to the effect observed with the α(−)R98N and α(−)R117Q substitutions (Fig. 3*A* and Table S1). The drastic effects exerted by mutations in the GluClα(−) side raised the question of whether mutations at the homologous positions in GluClβ would exert the same effects.

Contribution of the GluClβ Subunit to Glu Accommodation in Heteromeric GluClR Mutants. Sequence alignments (17, 23) indicate that the GluClβ subunit has identical residues at positions homologous to GluCl α(−)R98, α(−)R117, and α(−)S182. These residues are β(−)R66, β(−)R85, and β(−)S152, respectively (Fig. 3*E*). A 3D homology model built here for the α(+)/β(−) intersubunit interface (*SI Materials and Methods* and Fig. S4) predicts that these three β-subunit residues are sufficiently close to interact with Glu (Fig. 3*E*). However, heteromeric mutant receptors assembled of the αWT subunit, together with β(−)R66N, β(−)R85N, or β(−)S152A, did not display the drastic increase in Glu-EC_{50} typical of the homologous α-subunit mutants (Fig. 3*B* and Table S1). Most recently, Daeffler et al. (22) published a study where they investigated homomeric GluClβRs carrying a βT283S mutation in the pore-lining segments (see sequence with entry code Q17328 in the UniProtKB database). The latter mutation, per se, caused a dramatic improvement in the response to Glu (70-fold decrease in Glu-EC_{50}). Interestingly, when the βT283S mutation was combined with a β(−)S152A mutation (no. 126 in ref. 22), the Glu-EC_{50} relatively increased by 590-fold (22). Clearly, if the β-subunit (−) side were to contribute the "complementary" Glu-binding components in our heteromeric GluClαWT/βS152A receptor, we would have observed a much larger rightward shift of

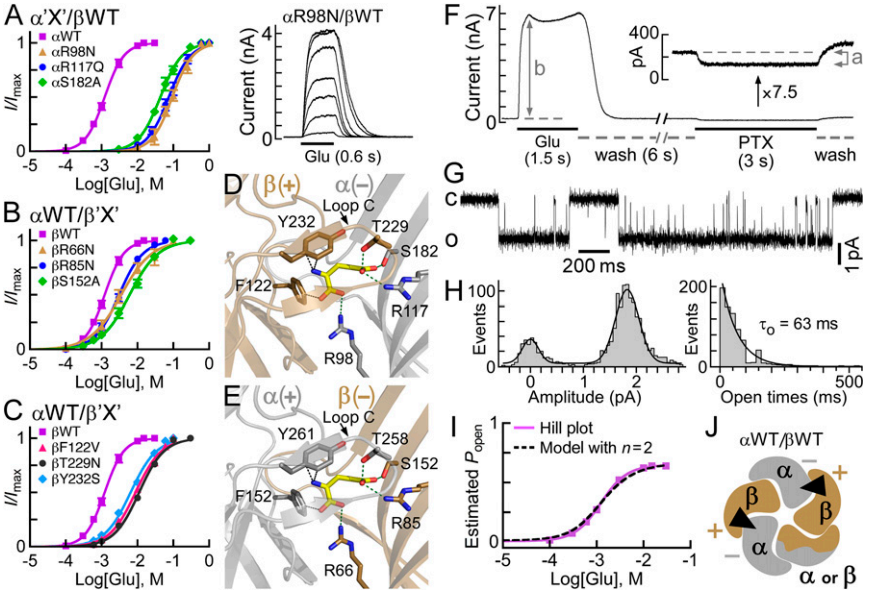

Fig. 3. Sensitivity to Glu of heteromeric GluClRs carrying single-site mutations within the putative Glu-binding pockets. (*A–C*) Dose–response curves plotted for the activation of various heteromeric receptors by Glu. Curves were fitted as described in Fig. 2 ($r^2 > 0.99$). Error bars correspond to SEM. "X" corresponds to mutations that were introduced in the GluClα(−) (*A*), GluClβ(−) (*B*), and GluClβ(+) (*C*) subunit sides. (*A*, *Right*) Representative current traces evoked by increasing Glu concentrations of 10 mM, 30 mM, 60 mM, 100 mM, 250 mM, 600 mM, and 1,000 mM in cells coexpressing the indicated GluClR subunits. Currents were measured at +60 mV. (*D* and *E*) Three-dimensional homology models of potential β(+)/α(−) and α(+)/β(−) intersubunit interfaces. Glu is shown with yellow-colored carbon atoms, whereas the carbons of receptor residues are colored in gray or gold for the α or β subunit, respectively. Oxygen and nitrogen atoms are colored in red and blue, respectively. Hydrogen atoms are not shown. Dotted green lines correspond to potential ion pairing or hydrogen bonding, whereas dotted black lines indicate distances compatible with van der Waals or cation–pi interactions. Loop C caps the putative Glu-binding pocket. (*F*) Representative current trace elicited by 15 mM Glu (saturating concentration) in cells expressing the GluClαWT/βWT receptor, followed by inhibition of the leak current by 200 μM picrotoxin (PTX). (*Inset*) Magnification (7.5-fold) of the trace observed upon PTX application. Measurements were performed at +80 mV. (*G*) Representative single-channel current recorded from a cell-attached patch containing the GluClαWT/βWT receptor. The pipette solution included 15 mM Glu (saturating concentration). The voltage command was −90 mV. The closed and open state levels are indicated by c and o, respectively. The single-channel $P_{o\text{-max}}$ is 0.64. (*H*, *Left*) Curve fitted to an event amplitude histogram by two Gaussian functions for the single-channel currents exemplified in *G*. The mean amplitude of the open state is 1.9 pA. (*H*, *Right*) Histogram of distribution of open times whose best-fit decay constant corresponds to the mean channel open time (τ_o). (*I*) Averaged dose–response data points of the GluClαWT/βWT receptor (purple squares) normalized to obtain the estimated P_{open} values that are plotted as a function of varying Glu concentrations. The purple line is the Hill curve. The dashed black line is the curve fitted based on an MWC allosteric model with two equivalent Glu-binding sites ($n = 2$) (Eq. **2**). (*J*) Plausible subunit arrangement of a heteromeric GluClRαWT/βWT receptor with two equivalent Glu-binding sites (black triangles), as viewed from the extracellular side.

the dose–response curve (complementary is defined in Fig. 1). Taken the results of the previous and current sections together, we infer that in the recombinant heteromeric receptors studied here, the GluClα(−) side, rather than the GluClβ(−) side, contributes the complementary components to Glu binding. Hence, we hypothesized that the GluClβ(+) side contributes the "principal" Glu-binding components in heteromeric GluClRs (principal is defined in Fig. 1).

To examine this hypothesis, we mutated residues β(+)F122, β(+)T229, and β(+)Y232 that might contact Glu, as predicted by sequence alignments (17, 23) and our 3D homology model (Fig. 3*D*). We then coexpressed the mutated β subunits (one at a time), together with the αWT subunit, and found that they shifted the dose–response curves rightward (Fig. 3*C*). Table S1 shows the extent of increase in the Glu-EC_{50} values, with the most prominent shift in the GluClαWT/βT229N and GluClαWT/βT229W receptors (by approximately eightfold compared with the GluClαWT/βWT receptor). We infer that the GluClβ(+) side in the heteromeric assemblies generated here contributes the principal Glu-binding components. Daeffler et al. (22) added to the homomeric GluClβT283S receptor a β(+)T229A mutation (no. 203 in ref. 22), which increased the Glu-EC_{50} to a much larger extent than observed here for the heteromeric GluClαWT/βT229N or GluClαWT/βT229W receptor. This difference can be attributed to the nature of the replacing amino acids. In the current study, we did not wish to change the chemical properties of the amino acids too much. This approach was adopted because the GluClαWT/βWT receptor inherently displays low affinity for Glu, which would probably make a dramatic increase in Glu-EC_{50} difficult to probe. Hence, we kept the capability of the replacing residues at position β(+)T229 to act as hydrogen bond donors (Asn, Trp) or a hydrogen bond acceptor (Asn). We expected that the greater size of the replacing residues would interfere with, but not abolish, Glu accommodation. This expectation emerged because position β(+)229 is located on loop C, which caps the putative Glu-binding pocket but, on the other hand, is considered to be flexible and mobile (46) (Fig. 3 *D* and *E*). As to the β(+)Y232S substitution, we probably eliminated a cation–pi interaction that was recently suggested to be formed in a homomeric GluClβR, between the β(+)Y232 aromatic ring and the α-amino nitrogen of Glu (22). Still, one cannot exclude hydrogen bonding between the hydroxyl group of the Ser we introduced at this position [β(+)232] and the α-amino nitrogen of Glu, which could explain the moderate effect of the β(+)Y232S mutation.

Stoichiometry of the Glu-Binding Sites in a Heteromeric WT GluClα/βR. The results presented in the previous sections suggest that a β(+)/α(−) intersubunit interface is involved in Glu accommodation; so, how many such functional interfaces exist per heteropentamer? The various single-site mutant receptors discussed so far share with the GluClαWT/βWT receptor Hill coefficients smaller than 2 but clearly larger than 1 (Table S1). This property suggests that there is more than one Glu-binding site per heteropentamer. To determine the number of functional sites and their microscopic equilibrium dissociation constants for Glu binding in the heteromeric GluClαWT/βWT receptor, we used an allosteric model based on the Monod–Wyman–Changeux (MWC) theory (47), as applied also by Karlin (48) to the nicotinic ACh receptor (nAChR) (reviewed in refs. 49 and 50). Because the GluClαWT/βWT receptor displays very slow and weak desensitization, we simplified the allosteric model by focusing on two major states as previously performed for weakly or nondesensitizing Cys-loop receptors such as: homomeric α7-nAChR mutants (51), homomeric α7-5HT_{3A}R chimeras (52), and heteromeric GABA receptors (53, 54). If the GluClαWT/βWT receptor has two equivalent (identical) Glu-binding sites, then Scheme I describes its MWC allosteric activation mechanism as follows:

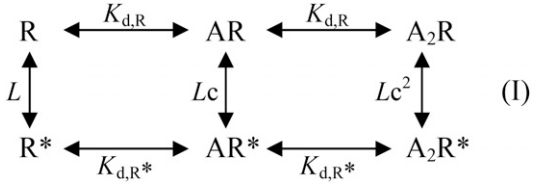

(I)

where R and R* are resting (closed) and active (open) receptor conformational states, respectively; A is an agonist molecule (Glu) that can complex with the receptor; $K_{d,R}$ and K_{d,R^*} are the microscopic equilibrium dissociation constants for agonist binding to the closed and open receptor states, respectively; and L is the equilibrium constant of the two receptor states (closed and open) in the absence of ligands. L is calculated by R/R* based on quantitative determinations, as follows.

Unoccupied R* corresponds to spontaneously open channels. Spontaneous activity (I_{spont}) was measured as the fraction of the leak current that could be blocked by picrotoxin, an ion-channel pore blocker of GluClRs (55) (e.g., Fig. 3*F*, indicated by "a"; elaborated in *SI Text*, section 2). Unoccupied R is estimated based on the current elicited by saturating Glu concentrations [maximal current response (I_{max})]. That is, I_{max} represents the activatable receptor population, which is at rest in the absence of Glu (Fig. 3*F*, indicated by "b"). However, I_{max} might not represent all of the activatable channels because not all of them are necessarily open at saturating Glu concentrations. Therefore, we determined the maximum open probability ($P_{o\text{-max}}$) of the ion channel by single-channel recordings at a saturating Glu concentration (Fig. 3 *G* and *H*) and then calculated R by $I_{max}/P_{o\text{-max}}$. Thus, $L = (I_{max}/P_{o\text{-max}})\cdot(1/I_{spont})$. Experimental $P_{o\text{-max}}$ and L values of three receptors are specified in Table S2 (footnotes).

I_{spont} and $P_{o\text{-max}}$ (0.64) were also used to normalize the dose–response data points of the GluClαWT/βWT receptor to estimate its open probability (P_{open}) at varying Glu concentrations by $[(I + I_{spont})/(I_{max} + I_{spont})]\cdot P_{o\text{-max}}$ (Fig. 3*I*). Then, to assess the applicability of Scheme I to the WT receptor activation mode, a curve was fitted to the normalized data points using an MWC allosteric model with two equivalent Glu-binding sites ($n = 2$) and the experimental mean L value (85) (Fig. 3*I*, dashed black curve and Eq. **2**). Table S2 provides the resulting K_d values (in bold). At very high Glu concentrations, the theoretical maximum open probability $P_{o\text{-max}}^* = 1/(1 + c^n L)$, where $c = K_{d,R^*}/K_{d,R}$ (54). So, when $n = 2$, the theoretical $P_{o\text{-max}}^* = 0.65$ for the GluClαWT/βWT receptor, which closely predicts the experimental $P_{o\text{-max}}$ (0.64). In contrast, fitting curves using an MWC model with other n values (one or equivalent three, four, or five Glu-binding sites; Eq. **2**) resulted in a theoretical $P_{o\text{-max}}^* \geq 0.68$ (Table S2). Moreover, analysis of the second-order Akaike information criterion difference (ΔAICc) (56) (*SI Materials and Methods*) selected the allosteric model with $n = 2$ as the most suitable MWC model for curve fitting in the GluClαWT/βWT receptor case (Table S2). Hence, we infer that the GluClαWT/βWT receptor has two functional equivalent Glu-binding sites. Taken together with the results shown in Fig. 3 *A*–*C*, we suggest that these two Glu-binding sites likely lie at two β(+)/α(−) intersubunit interfaces (Fig. 3*J*). Although one cannot absolutely exclude the possibility of a change in subunit stoichiometry due to mutations, we argue that such a change is unlikely to occur here (*SI Text*, section 3, Fig. S5, and Table S3).

Mutation in the IVM-Binding Pocket Gives Rise to a Third Glu-Binding Site. During our research, we identified a mutation in the putative IVM-binding site (αL279W; position α(−)L218 in GluClα_{cryst}R) that decreased the Glu-EC_{50} of the GluClαL279W/βWT receptor by ~25-fold, compared with the GluClαWT/βWT receptor

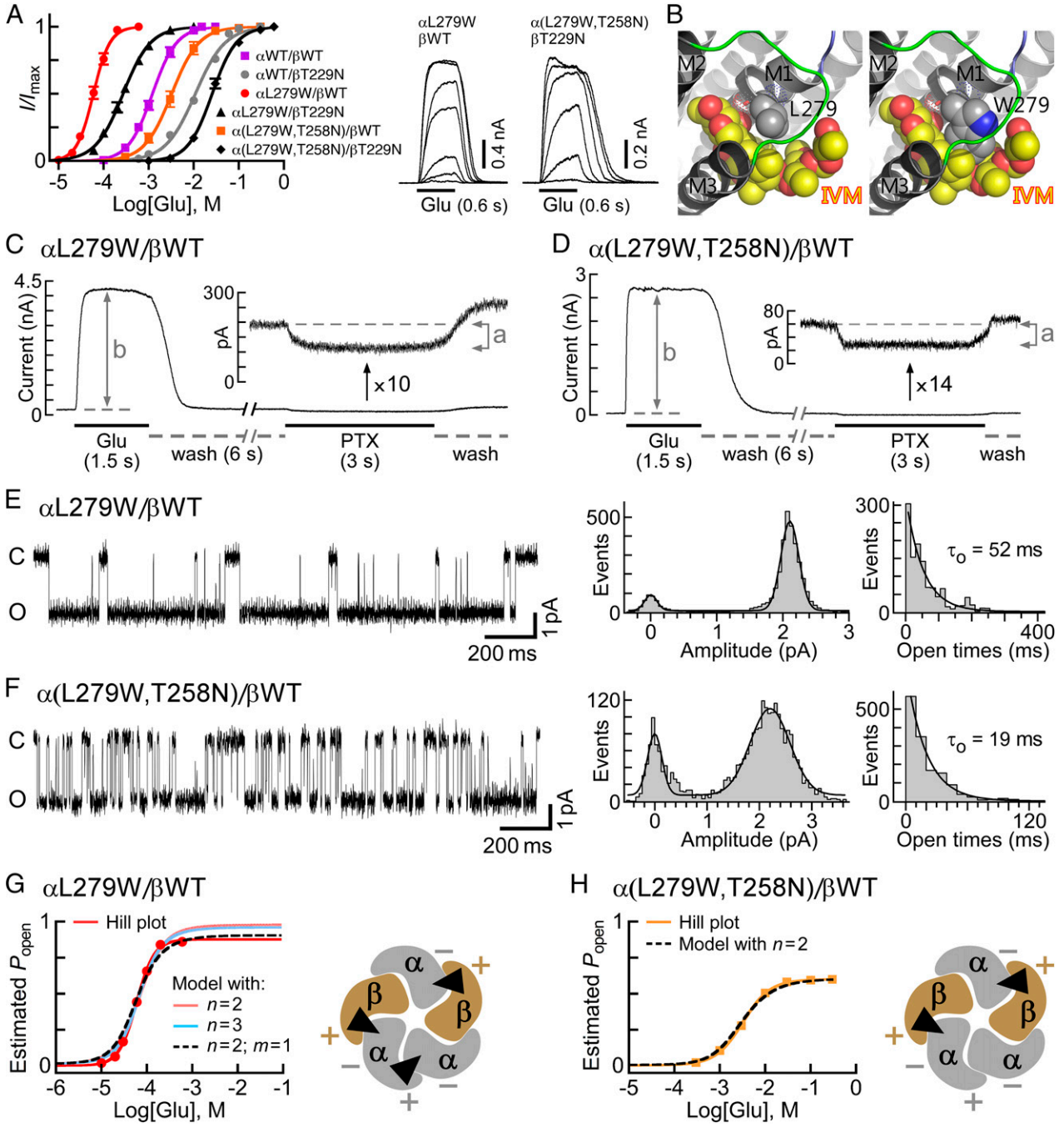

Fig. 4. Subunit stoichiometry and arrangement in heteromeric GluClα/βR mutants. (*A*, *Left*) Glu dose–response curves plotted for the activation of receptors consisting of the indicated subunits. Curves were fitted as described in Fig. 2*B* ($r^2 > 0.99$). Error bars correspond to SEM. (*A*, *Right*) Representative current traces evoked by applying increasing Glu concentrations on cells cotransfected with the indicated receptor subunits. Glu concentrations: 0.01 mM, 0.02 mM, 0.03 mM, 0.06 mM, 0.1 mM, 0.2 mM, and 0.3 mM (for the αL279W/βWT receptor) and 3 mM, 10 mM, 30 mM, 100 mM, 300 mM, and 600 mM [for the α(L279W, T258N)/βT229N receptor]. Currents were measured at +60 mV. (*B*) Three-dimensional models of the IVM-binding pocket at an α(+)/α(−) intersubunit interface. (*Left*) Side chain of the native αL279, which does not interact with IVM. (*Right*) Side chain of the substituting Trp, which potentially forms multiple van der Waals interactions with the lactone backbone of IVM. Side chains are shown as gray (carbon atoms) and blue (nitrogen) spheres. IVM is shown as yellow (carbon atoms) and red (oxygen atoms) spheres. Hydrogen atoms were removed for better viewing. The PDB 3RIF structure was used for generating the αL279W mutant and the pictures. (*C* and *D*) Representative current traces elicited by saturating concentrations of Glu in cells cotransfected with the indicated subunits (0.5 mM and 30 mM Glu in *C* and *D*, respectively). (*Insets*) Magnifications for the effect of picrotoxin (PTX; 200 μM) are shown. (*E* and *F*) Representative single-channel currents recorded in cell-attached patches from cells cotransfected with the indicated receptor subunits. The pipette solution included saturating Glu concentrations (0.5 mM and 30 mM Glu in *E* and *F*, respectively). The voltage command was −90 mV. The closed and open state levels are indicated by c and o, respectively. $P_{o\text{-max}}$ values are 0.86 and 0.60 for the receptors indicated in *E* and *F*, respectively. On the right side of each current trace shown are curves fitted to event histograms plotted as described in Fig. 3*H*; they provide mean amplitudes of 2.1 pA and 2.2 pA for the open states of the receptors indicated in *E* and *F*, respectively. Mean channel open times (τ_o) are indicated inside the rightmost panels. (*G* and *H*) Estimated P_{open} plotted as a function of varying Glu concentrations. Red and orange lines correspond to the Hill curves. Other curves were plotted based on an MWC allosteric model using Eq. **2** for cases with either two ($n = 2$) or three ($n = 3$) equivalent Glu-binding sites or, alternatively, Eq. **3** for a case with two equivalent and a third distinct Glu-binding sites ($n = 2$, $m = 1$). (*G* and *H*, *Right*) Plausible subunit arrangements with intersubunit Glu-binding sites (black triangles), as viewed from the extracellular side.

(Fig. 4*A* and Table S1). This mutation increased the Hill coefficient to 2.6, suggesting that the number of occupiable Glu-binding sites in the receptor mutant is probably not less than three. Intrigued by this possibility, we initially examined an MWC allosteric model with either two or three equivalent Glu-binding sites. To this end, we determined the values of I_{spont}, I_{max}, $P_{o\text{-}max}$, and L for the GluClαL279W/βWT receptor [Fig. 4 *C* and *E* and Table S2 (footnotes)] and estimated its P_{open} at varying Glu concentrations, all as described above for the GluClαWT/βWT receptor. Then, a curve was fitted to the normalized dose–response data points using an MWC allosteric model with $n = 2$ and the experimental mean L value (81) (Fig. 4*G*, salmon-colored curve and Eq. **2**). The resulting K_d values (Table S2, same line of "2, 0") were applied to calculate the theoretical $P_{o\text{-}max}{}^*$ by $1/(1 + c^2L) = 0.98$, which turned out to be much higher than the experimental $P_{o\text{-}max}$ (0.86). Extrapolating the salmon-colored curve in Fig. 4*G* (model with $n = 2$) until the theoretical $P_{o\text{-}max}{}^*$ is reached indicates a strong deviation of this curve from the Hill plot at high Glu concentrations. Alternatively, a curve was fitted to the normalized dose–response data points using an MWC allosteric model with three equivalent Glu-binding sites ($n = 3$) and the same L value (81) (Fig. 4*G*, cyan-colored curve and Eq. **2**). The resulting K_d values (Table S2, same line of "3, 0") were used to calculate the theoretical $P_{o\text{-}max}{}^*$ by $1/(1 + c^3L) = 0.96$, which is also much higher than the experimental $P_{o\text{-}max}$ (0.86). Extrapolation of the cyan-colored curve in Fig. 4*G* (model with $n = 3$) until the theoretical $P_{o\text{-}max}{}^*$ is reached indicates a strong deviation of this curve from the Hill plot at high Glu concentrations. Curve fitting with other values for n (one, or equivalent four or five Glu-binding sites) resulted in a theoretical $P_{o\text{-}max}{}^* \geq 0.95$ (Table S2). We therefore applied an MWC allosteric model with two equivalent and a third distinct Glu-binding sites ($n = 2$, $m = 1$), using the same L value (81) (Fig. 4*G*, dashed black curve and Eq. **3**). In this case, $K_{d,R}$ and K_{d,R^*} characterize the two equivalent Glu-binding sites in the closed and open states, respectively; and $K'_{d,R}$ and K'_{d,R^*} characterize the third Glu-binding site in the closed and open states, respectively [Table S2 (in bold)]. Scheme II describes the MWC allosteric mechanism that corresponds to the GluClαL279W/βWT receptor:

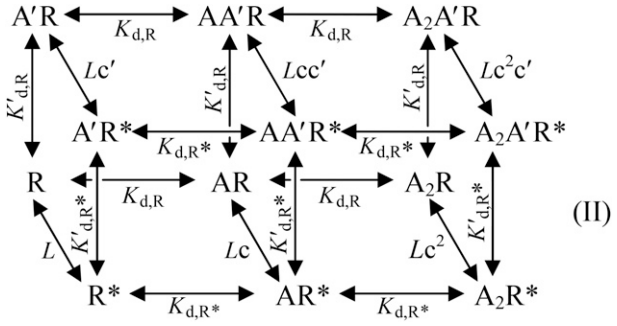

where $c = K_{d,R^*}/K_{d,R}$ and $c' = K'_{d,R^*}/K'_{d,R}$. In this case, the theoretical $P_{o\text{-}max}{}^* = 1/(1 + c^n c'^m L) = 1/(1 + c^2 c'^1 L) = 0.89$, which is much closer to the experimental $P_{o\text{-}max}$ (0.86) than in cases of curve fitting with other numbers of Glu-binding sites (Table S2). Analysis of the ΔAICc selected the allosteric model with two equivalent and a third distinct Glu-binding sites ($n = 2$, $m = 1$) as the most appropriate MWC model for curve fitting in the GluClαL279W/βWT receptor case (Table S2).

The allosteric mechanism suggested above does not provide details regarding the subunit types that form the third Glu-binding site interface in the GluClαL279W/βWT receptor, however. If the fifth subunit is GluClβ, then it will give rise to α(+)/β(−) and β(+)/β(−) intersubunit interfaces (envisioned in Fig. 3*J*); however, based on the aforementioned results, the GluClβ(−) side is less likely to contribute to Glu binding. If the fifth subunit is GluClα, then it will give rise to α(+)/α(−) and α(+)/β(−) intersubunit interfaces (envisioned in Fig. 4*G*, *Right*); so, the α(+)/α(−) intersubunit interface remains a reasonable candidate to form the third Glu-binding site. However, this working hypothesis required further experimental investigation. Because the GluClα(−) side was inferred to line the two Glu-binding pockets (Fig. 3 and main text), we introduced an α(+)T258N mutation (in loop C), in addition to the αL279W mutation. The homologous mutation [β(+)T229N] in the GluClαWT/βT229N receptor was shown to increase the Glu-EC_{50} by approximately eightfold, compared with the GluClαWT/βWT receptor (Fig. 3*C* and Table S1; presented again in Fig. 4*A* in gray for convenience). Hence, an α(+)T258N mutation was anticipated to affect a potential α(+)/α(−) intersubunit Glu-binding site, without directly interfering with Glu binding at the two β(+)/α(−) sites. Fig. 4*A* shows that the dose–response curve of the GluClα (L279W,T258N)/βWT receptor is significantly shifted to the right relative to the curve of the GluClαL279W/βWT receptor, with an ∼57-fold increase in the Glu-EC_{50} and a decrease of the Hill coefficient to $n_H = 1.6$ (Table S1). These macroscopic properties resemble the properties displayed by the GluClαWT/βWT receptor, which has two equivalent Glu-binding sites.

To quantify the effect of the α(+)T258N mutation further, we determined the values of I_{spont}, I_{max}, $P_{o\text{-}max}$, and L for the GluClα (L279W,T258N)/βWT receptor [Fig. 4 *D* and *F* and Table S2 (footnotes)] and estimated its P_{open} at varying Glu concentrations, all as described above for the GluClαWT/βWT receptor. Then, a curve was fitted to the normalized dose–response data points using an MWC allosteric model with two equivalent Glu-binding sites ($n = 2$) and the experimental mean L value (203) (Fig. 4*H*, dashed black curve and Eq. **2**). The resulting K_d values are provided in Table S2 (in bold). The theoretical and experimental maximum open probabilities were found to be equal (0.60), whereas other values for n (one, or equivalent three, four, or five Glu-binding sites) resulted in higher theoretical $P_{o\text{-}max}{}^*$ values (Table S2). In addition, the analysis of the ΔAICc selected the allosteric model with $n = 2$ as the most suitable MWC model for curve fitting in the GluClα(L279W,T258N)/βWT receptor case (Table S2). Hence, the results imply that this double-mutant receptor lost the third Glu-binding site, and its remaining two equivalent Glu-binding sites display slightly lower affinity for Glu than the GluClαWT/βWT receptor [Table S2 (in bold)]. Provided that the mutations have not changed the subunit stoichiometry (as argued in *SI Text*, section 3), the two Glu-binding sites of the GluClα(L279W,T258N)/βWT receptor likely lie at β(+)/α(−) intersubunit interfaces (Fig. 4*H*, *Right*). As discussed above, the GluClβ(−) side is less likely to contribute to Glu binding, and so is an α(+)/β(−) intersubunit interface. We therefore infer that the α(+)T258N mutation is likely located at an α(+)/α(−) intersubunit interface. Taken together, our results suggest that in the GluClαL279W/βWT receptor, an α(+)/α(−) intersubunit interface likely forms a third Glu-binding site (Fig. 4*G*, *Right*), whereas Glu binding to this interface is impaired by adding the α(+)T258N mutation (Fig. 4*H*, *Right*).

β(+)T229N is the homologous mutation of α(+)T258N. Combining the αL279W mutation with the β(+)T229N mutation, to give a GluClαL279W/βT229N receptor, led to a fivefold rightward shift of the dose–response curve relative to the GluClαL279W/βWT receptor (Fig. 4*A* and Table S1). This shift is much smaller than the 57-fold rightward shift observed in the GluClα(L279W, T258N)/βWT receptor relative to the GluClαL279W/βWT receptor (Fig. 4*A* and Table S1). This difference is in line with the above conclusion that an α(+)/α(−) intersubunit interface forms the third Glu-binding site in the GluClαL279W/βWT receptor.

Interestingly, the α(+)T258N mutation in the GluClα(L279W, T258N)/βWT receptor has not only eliminated the third α(+)/α(−) intersubunit Glu-binding site but also considerably decreased the

Glu-binding affinity of the two equivalent β(+)/α(−) interfaces relative to the GluClαL279W/βWT receptor [Table S2 (in bold)]. We suggest that the mutation in the (+) side of the plausible α(+)/α(−) Glu-binding site interface could allosterically affect the other Glu-binding site interfaces. Combining all three mutations to produce a GluClα(L279W,T258N)/βT229N receptor shifted the dose–response curve by 455-fold rightward relative to the GluClαL279W/βWT receptor (Fig. 4*A* and Table S1). This rightward shift is larger by ∼90-fold than the fivefold rightward shift observed for the GluClαL279W/βT229N receptor, which suggests that also in the triple mutant, the α(+)/α(−) intersubunit interface has a strong allosteric relationship with the β(+)/α(−) Glu-binding site interfaces. Notably, the Hill coefficient decreased from n_H = 2.6 in the GluClαL279W/βWT receptor to n_H = 1.5 in the GluClαL279W/βT229N receptor (Table S1), suggesting that the β(+)T229N mutation exerts a reciprocal allosteric effect on the third α(+)/α(−) intersubunit interface.

Effect of the αL279W Mutation on the Responsiveness of the Heteromeric GluClαL279W/βWT Receptor to IVM. The crystal structure of the homomeric GluClα_{cryst}R indicates that the backbone carbonyl oxygen of αL279 (L218 in GluClα_{cryst}R) forms a hydrogen bond with hydroxyl O13-H of IVM, whereas the αL279 side chain does not interact with IVM (23) (Fig. 4*B*, *Left*). Three-dimensional homology modeling predicts that a Trp side chain introduced at position α279 might form multiple contacts with IVM (Fig. 4*B*, *Right*). If so, how might this mutation affect the responsiveness of the GluClαL279W/βWT receptor to IVM? To answer this question, we had to determine the IVM EC_{50} for the WT and mutant receptors. However, unlike the fully reversible responses to Glu, after activation by IVM, the response could not be reproduced by reapplication of IVM even when the first IVM application was followed by a long-term wash (up to 30 min). Other groups also observed this phenomenon when the wash was applied for several minutes (13) or an hour (18). Hence, to quantify the effect of the mutation, we first used the methodology of Lester and coworkers (18) to determine the time constant of conductance development following IVM application. To this end, voltage ramps were carried out during the application of various IVM concentrations, with each application in a different cell. Fig. 5*A* shows an example of such an experiment. Superimposition of the output currents of the voltage ramps shows a sharp increase in slopes that reflects the robust IVM-induced conductance and a clear leftward shift (decrease) of the reversal potential that occurs mainly after the conductance reached its maximum (Fig. 5*B*). The shift of the reversal potential indicates a change in the Nernst potential for Cl^-

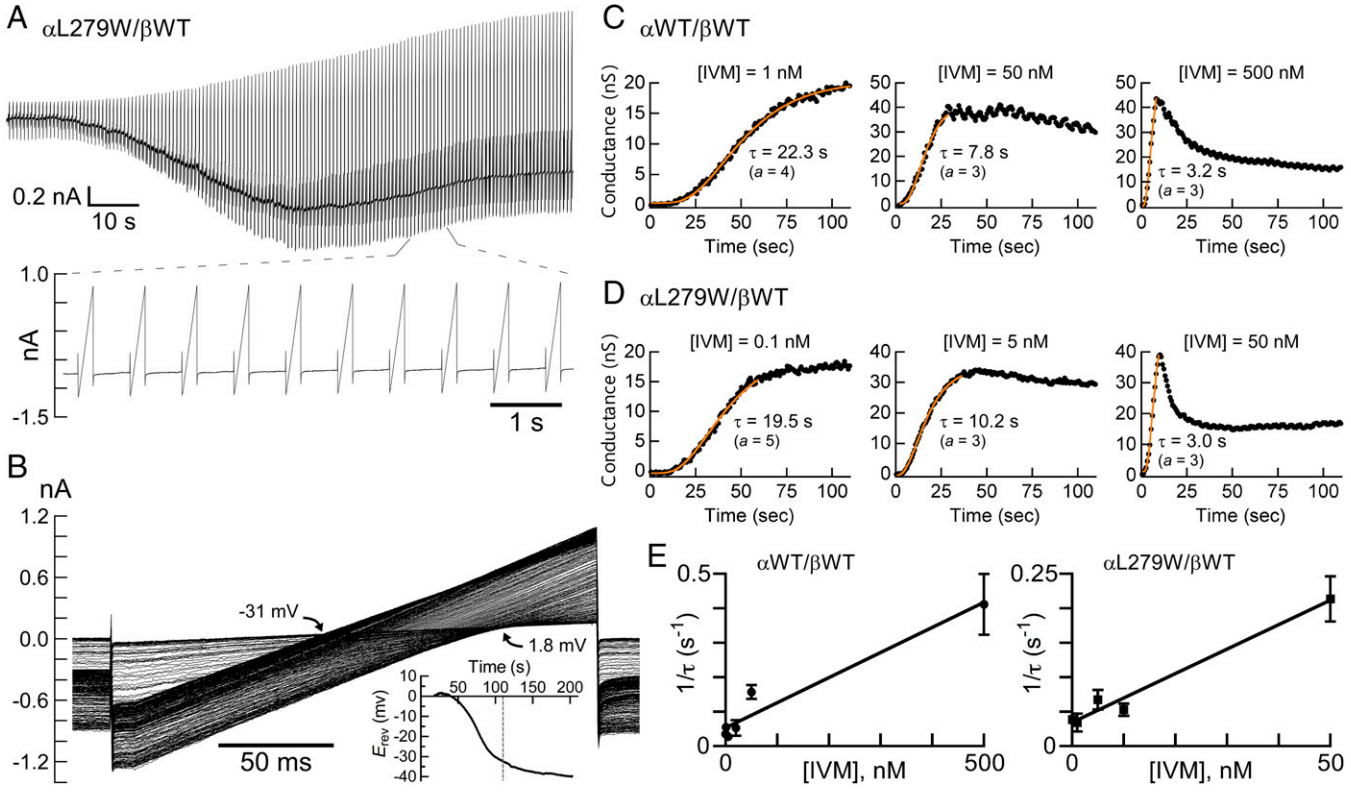

Fig. 5. Affinity of WT and mutant heteromeric GluClRs for IVM. (*A*) Representative current trace elicited by 0.1 nM IVM in a cell coexpressing the indicated receptor subunits. IVM was applied throughout the entire time of the recording (210 s), which was made at −60 mV with intervening 200-ms-long voltage ramps from −80 mV to +20 mV as described in *SI Materials and Methods*. Note that only the output currents of the first 152 (of 290) voltage ramps are shown for clarity and the lower part shows a magnification of some output currents. (*B*) Superimposition of the output currents corresponding to the first 152 voltage ramps shown in *A*. Black arrows indicate the reversal potential (E_{rev}) span for the first 152 output currents of the voltage ramps. (*Inset*) Decrease in the E_{rev} throughout the entire recording time. The dotted line marks 110 s, which is the time recording of the output currents of the first 152 voltage ramps. (*C* and *D*) Chloride conductance as a function of time in different representative cells. The points corresponding to the conductance (in black) were determined based on the output currents of the voltage ramps (main text and *SI Materials and Methods*). To determine the time constants of conductance development (τ), exponential curves (orange) were fitted to the conductance points with a nonlinear regression using Eq. **S2**, with varying *"a"* values to account for the sigmoid time course. Note that the cell shown in the leftmost panel of *D* under 0.1 nM IVM, is the same cell shown in *A* and *B*. (*E*) Points corresponding to the averaged 1/τ plotted as a function of IVM concentrations. Curves were fitted to the data points by linear regression. The lowest IVM concentration was 0.1 nM for both the WT and mutant receptors. Forty-nine and 32 cells were analyzed as described throughout this figure to obtain the left (r^2 = 0.95) and right (r^2 = 0.98) graphs, respectively. Error bars correspond to SEM.

and in the electrochemical driving force acting on Cl^- ions. The chloride conductance is defined by the slope of the current–voltage (I/V) relations extracted from the output currents of the voltage ramps, and could be determined at several membrane voltage spans. Fig. S6*A* shows the slope conductance determined between −75 mV and −65 mV, around the reversal potential, and between +10 mV and +20 mV, as a function of time. The rise time of the conductance increment was found to be similar for all of the three aforementioned voltage spans (Fig. S6*A*). Notably, during the applications of high IVM concentrations, the conductance rise was followed by a decrease in the conductance to a steady state in all voltage spans and in both the WT and indicated mutant receptors (Fig. S6*A*). Because the current decay under high IVM concentrations was faster at −65 mV than at +20 mV (Fig. S6*B*), and because the exponential fits of the conductance rise time were very similar at the different membrane voltage spans, we chose to analyze the conductance development further between +10 mV and +20 mV. Fig. 5 *C* and *D* shows the development of the conductance under the application of different IVM concentrations in different representative cells.

The exponential fits of the conductance rise time (e.g., Fig. 5 *C* and *D*, orange curves) provide the time constant of conductance development (τ), whose reciprocal ($1/\tau$) increased linearly with the increase in IVM concentration (Fig. 5*E*). Because IVM does not readily dissociate from the receptor (13, 18) and the number of possible intermediate IVM-bound closed states is not known, the simplest possible kinetic model that could describe the activation mechanism by IVM would be one in which the channel opens when IVM binds and closes after a very long time when IVM dissociates. Scheme III describes this kinetic model:

$$\text{IVM} + \text{R} \underset{k_b}{\overset{k_f}{\rightleftharpoons}} \text{IVM•R}^* \qquad \text{(III)}$$

where R is the unoccupied closed receptor, IVM·R* is the IVM-bound open receptor, and $1/\tau = k_f\,[\text{IVM}] + k_b$. The slope of the curves in Fig. 5*E* corresponds to the IVM association rate constant (k forward, k_f). The IVM dissociation rate constant (k backward, k_b) is the extrapolated intercept of the linear curve with the y axis in Fig. 5*E*. The apparent K_d would be k_b/k_f, giving 73×10^{-9} M for IVM binding to the GluClαWT/βWT receptor ($k_b = 5.3 \times 10^{-2}$ s^{-1} and $k_f = 7.3 \times 10^5$ $s^{-1}{\cdot}M^{-1}$). In contrast, the apparent K_d for IVM binding to the GluClαL279W/βWT receptor was 9.7×10^{-9} M ($k_b = 3.4 \times 10^{-2}$ s^{-1} and $k_f = 3.5 \times 10^6$ $s^{-1}{\cdot}M^{-1}$), which indicates that the affinity of the mutant receptor for IVM is 7.5-fold higher than the affinity of the WT receptor for IVM. Note that because no experiments revealed that IVM could be washed out of the receptor (13, 18), the k_b values are expected to be on the order of $<10^{-4}$ s^{-1}. However, the values here were found to be on the order of 10^{-2} s^{-1}, implying that IVM should be removable. We therefore cannot exclude the possibility that after opening of the GluClR ion channel by IVM, a subsequent conformational change leads to trapping of IVM between the transmembrane helices irreversibly.

Discussion

To determine unequivocally the subunit stoichiometry and arrangement in native GluClα/βRs, high-resolution X-ray crystallography of heteropentameric receptors purified from the organisms that naturally express them is necessary. To the best of our knowledge, such a determination is yet out of reach. Hence, an alternative methodology must be considered. In Cys-loop receptors, the neurotransmitter-binding pockets lie at the interface between adjacent subunits (1–9). One could therefore use site-specific mutagenesis and biophysical characterization of activation mechanisms in recombinant receptors to find the types of subunits that line the agonist-binding pockets. By working with recombinant receptors, however, one cannot exclude the possibility that the ratio of subunit cDNA transfected, the type of the expressing cell, or a mutation might influence the receptor's subunit composition (e.g., 45, 57, 58). We nevertheless argue that the specific mutations we introduced are less likely to change the subunit stoichiometry of the recombinant receptors studied here (*SI Text*, section 3).

In various Cys-loop receptors, the β1β2, Cys, and β8β9 loops were shown to play a key role in transducing the agonist-binding energy into ion-channel gating force (35–44). Here, we first demonstrated that although the homomeric GluClαR is not responsive to Glu, the β1β2, Cys, and β8β9 loops of the GluClα subunit are fully capable of coupling Glu binding to channel gating in a heteromeric GluClα/β microchimera that has the sequences of the α-subunit loops. Subsequently, we undertook to identify the intersubunit interfaces involved in Glu accommodation by heteromeric GluClα/βRs. Taking advantage of the crystal structure of a truncated homomeric $\text{GluCl}\alpha_{\text{cryst}}\text{R}$ as a template, we built a 3D homology model for the GluClβ subunit. Then, based on the two structures, we introduced single-site mutations in the (−) side of either the GluClα subunit or the GluClβ subunit at positions carrying residues that putatively interact with Glu. Characterization of the effects of these mutations on the receptor function allowed us to suggest that in the heteromeric GluClα/βRs studied here, the (−) side of the α subunit, rather than the (−) side of the β subunit, contributes complementary components to Glu binding. Single-site mutations and functional analysis of heteromeric GluClα/βRs carrying mutations in the (+) side of the β subunit imply that this side contributes principal components to Glu binding.

When considering the GluClαWT/βWT receptor in terms of the MWC allosteric mechanism, we infer that a maximum of two equivalent binding sites can be occupied by Glu [Fig. 3*I*, Scheme I, and Table S2 (in bold)]. Provided that the aforementioned single-site mutations introduced at the intersubunit interfaces have not changed the subunit stoichiometry (as argued in *SI Text*, section 3), Glu binding likely takes place at two β(+)/α(−) intersubunit interfaces. Hence, one can envision a subunit arrangement as illustrated in Fig. 3*J* for a recombinant GluClαWT/βWT receptor expressed in CHO cells, with no information regarding the type of the fifth subunit.

When considering the GluClαL279W/βWT receptor in terms of the MWC allosteric mechanism, we infer that Glu can occupy three sites (Fig. 4*G* and Scheme II). These sites are (*i*) two equivalent Glu-binding sites that are likely located at β(+)/α(−) intersubunit interfaces and display considerably higher affinity for Glu than their homologous binding sites in the GluClαWT/βWT receptor and (*ii*) a third distinct site with slightly lower Glu-binding affinity, in both the resting (closed) and active (open) receptor states [Table S2 (in bold)]. We argue that the third Glu-binding site is formed between two adjacent α subunits; the arguments for that conclusion are as follows:

i) In CHO cells, a WT GluClβ subunit does not assemble into a homopentamer capable of responding to Glu or IVM, which indicates that the β subunit has difficulties in creating Glu-binding β(+)/β(−) intersubunit interfaces (Fig. S2*A* and Table S1).

ii) In the heteromeric GluClα/βRs studied here, three single-site mutations in the β(−) side did not lead to drastic effects on the receptor activation by Glu, unlike the case of the same mutations introduced at the homologous positions in the α(−) side.

iii) The homomeric GluClαL279W receptor responds to very high Glu concentrations (Fig. S7), indicating the capability of an α(+)/α(−) intersubunit interface to accommodate Glu (with no need for IVM prebinding).

iv) Adding a mutation in loop C (+ side) of the αL279W subunit gave rise to an α(L279W,T258N)/βWT receptor that lost the third Glu-binding site (Fig. 4*H*), whereas the remaining two equivalent Glu-binding sites display microscopic equilibrium dissociation constants slightly higher than the microscopic equilibrium dissociation constants of the GluClαWT/βWT receptor [Table S2 (in bold)].

A third Glu-binding site located at an α(+)/α(−) intersubunit interface requires that the fifth subunit would be a GluClα subunit. We therefore suggest that the subunits of the recombinant heteromeric GluClα/βRs studied here assemble in an anticlockwise β-α-β-α-α fashion, as viewed from the extracellular side (Fig. 4 *G* and *H*, *Right*). Notably, previous studies show that expressing the heteromeric α4β2 nAChR under conditions that favor an $(\alpha4\beta2)_2\alpha4$ stoichiometry (three α4 and two β2 subunits) results in a receptor having two α4(+)/β2(−) interfaces with high agonist sensitivity and a third binding site at the α4(+)/α4(−) interface that displays low agonist sensitivity (59–61).

As discussed in *Results*, the function of heteromeric receptors containing the αL279W mutation, together with a Thr→Asn substitution in loop C of the α subunit, β subunit, or both subunits, suggests that the two intersubunit interface types, α(+)/α(−) and β(+)/α(−), likely affect each other allosterically. Possible structural reasons for this mutual allosteric influence are provided in *SI Text*, section 4. Interestingly, an allosteric relationship between different extracellular intersubunit interfaces was proposed for the heteromeric α1β2γ2 $GABA_A$ receptor (62). In the latter case, conformational movements induced by benzodiazepine binding at the α/γ extracellular interface were suggested to propagate across the α1 subunit to the β/α GABA-binding site interface (62).

In the $GluCl\alpha_{cryst}R$, L218 (αL279 in the full-length subunit used here) is part of the IVM-binding pocket located between M1 and M3 of adjacent subunits (23) (Fig. 4*B*, *Left*). The clear increase in the affinity of the GluClαL279W/βWT receptor for IVM (Fig. 5*E*; 7.5-fold) implies that the IVM-binding pockets of the heteromeric receptor are homologous to the IVM-binding pockets of the homomeric $GluCl\alpha_{cryst}R$. The structural mechanism underlying the effect of the αL279W mutation in the IVM-binding site is not clear. However, the microscopic equilibrium dissociation constants for Glu binding determined here imply that the conformational change induced by this mutation in the IVM-binding pocket propagates to the Glu-binding pockets and affects their affinity for Glu. It is not known whether Glu and IVM induce the same conformational change in the coupling loops. In the heteromeric α1β2γ2 $GABA_A$ receptor, for example, it was demonstrated that positive benzodiazepine modulators induce movements in loop F (β8β9 loop) of the γ2 subunit near the transmembrane channel domain (63). Such movements were not triggered by the binding of GABA, the allosteric modulator pentobarbital, or the inverse agonist methyl-6,7-dimethoxy-4-ethyl-β-carboline-3-carboxylate (63).

In conclusion, our study provides evidence that the *C. elegans* heteromeric GluClR contains three α subunits and two β subunits arranged in an anticlockwise β-α-β-α-α fashion, as viewed from the extracellular side, with two Glu-binding sites located at the β(+)/α(−) intersubunit interfaces. The α(+)/α(−) intersubunit interface creates a third "dormant" Glu-binding site that becomes functional upon a conformational change induced by a mutation in the IVM-binding pocket.

Materials and Methods

Additional experimental procedures and data analyses are described in *SI Materials and Methods*.

Data analysis and mathematical modeling were performed using the Clampfit 10 program implemented in pClamp 10, and GraphPad Prism software.

Dose–response curves were fitted to the data points by a nonlinear regression using the Hill equation (Eq. **1**):

$$\frac{I}{I_{max}} = \frac{1}{1 + 10^{(\log EC_{50} - \log[Glu])n_H}}, \quad [1]$$

where I is the current response, I_{max} is the maximal current response, EC_{50} is the agonist effective concentration that elicits 50% of the maximal current response, [Glu] is the concentration of Glu, and n_H is the Hill coefficient.

For the allosteric modeling, Eq. **2** was used:

$$P_{open} = \frac{1}{1 + L\left\{\frac{1 + [Glu]/K_{d,R}}{1 + [Glu]/K_{d,R*}}\right\}^n}, \quad [2]$$

where P_{open} is the open probability estimated at varying Glu concentrations (54) (main text). [Glu] is the concentration of the agonist (Glu) for which there are n equivalent binding sites, each with a microscopic equilibrium dissociation constant of $K_{d,R}$ in the resting (closed) state and $K_{d,R*}$ in the active (open) state. L is the equilibrium constant of the two states in the absence of ligands. The L values were determined by functional experiments, as described in the main text.

For a receptor phenotype that does not behave as a receptor having only n equivalent Glu-binding sites, Eq. **3** [cf. Karlin (48)] was used:

$$P_{open} = \frac{1}{1 + L\left\{\frac{1 + [Glu]/K_{d,R}}{1 + [Glu]/K_{d,R*}}\right\}^n \left\{\frac{1 + [Glu]/K'_{d,R}}{1 + [Glu]/K'_{d,R*}}\right\}^m}, \quad [3]$$

where m is the number of sites that Glu binds with microscopic equilibrium dissociation constants, $K'_{d,R}$ in the closed state and $K'_{d,R*}$ in the open state.

ACKNOWLEDGMENTS. We thank H. A. Lester for providing us with the initial GluClα subunit construct.

1. Karlin A (2002) Emerging structure of the nicotinic acetylcholine receptors. *Nat Rev Neurosci* 3(2):102–114.
2. Lester HA, Dibas MI, Dahan DS, Leite JF, Dougherty DA (2004) Cys-loop receptors: New twists and turns. *Trends Neurosci* 27(6):329–336.
3. Betz H, Laube B (2006) Glycine receptors: Recent insights into their structural organization and functional diversity. *J Neurochem* 97(6):1600–1610.
4. Sine SM, Engel AG (2006) Recent advances in Cys-loop receptor structure and function. *Nature* 440(7083):448–455.
5. Taylor P, et al. (2007) Structure-guided drug design: Conferring selectivity among neuronal nicotinic receptor and acetylcholine-binding protein subtypes. *Biochem Pharmacol* 74(8):1164–1171.
6. Olsen RW, Sieghart W (2008) International Union of Pharmacology. LXX. Subtypes of gamma-aminobutyric acid(A) receptors: Classification on the basis of subunit composition, pharmacology, and function. Update. *Pharmacol Rev* 60(3):243–260.
7. Changeux JP (2010) Allosteric receptors: From electric organ to cognition. *Annu Rev Pharmacol Toxicol* 50:1–38.
8. Thompson AJ, Lester HA, Lummis SC (2010) The structural basis of function in Cys-loop receptors. *Q Rev Biophys* 43(4):449–499.
9. Lynagh T, Lynch JW (2012) Molecular mechanisms of Cys-loop ion channel receptor modulation by ivermectin. *Front Mol Neurosci* 5:60.
10. Crump A, Ōmura S (2011) Ivermectin, 'wonder drug' from Japan: The human use perspective. *Proc Jpn Acad, Ser B, Phys Biol Sci* 87(2):13–28.
11. Campbell WC (2012) History of avermectin and ivermectin, with notes on the history of other macrocyclic lactone antiparasitic agents. *Curr Pharm Biotechnol* 13(6): 853–865.
12. Geary TG (2005) Ivermectin 20 years on: Maturation of a wonder drug. *Trends Parasitol* 21(11):530–532.
13. Cully DF, et al. (1994) Cloning of an avermectin-sensitive glutamate-gated chloride channel from Caenorhabditis elegans. *Nature* 371(6499):707–711.
14. Etter A, Cully DF, Schaeffer JM, Liu KK, Arena JP (1996) An amino acid substitution in the pore region of a glutamate-gated chloride channel enables the coupling of ligand binding to channel gating. *J Biol Chem* 271(27):16035–16039.
15. Dent JA, Davis MW, Avery L (1997) avr-15 encodes a chloride channel subunit that mediates inhibitory glutamatergic neurotransmission and ivermectin sensitivity in Caenorhabditis elegans. *EMBO J* 16(19):5867–5879.
16. Vassilatis DK, et al. (1997) Genetic and biochemical evidence for a novel avermectin-sensitive chloride channel in Caenorhabditis elegans. Isolation and characterization. *J Biol Chem* 272(52):33167–33174.
17. Li P, Slimko EM, Lester HA (2002) Selective elimination of glutamate activation and introduction of fluorescent proteins into a Caenorhabditis elegans chloride channel. *FEBS Lett* 528(1-3):77–82.
18. Slimko EM, McKinney S, Anderson DJ, Davidson N, Lester HA (2002) Selective electrical silencing of mammalian neurons in vitro by the use of invertebrate ligand-gated chloride channels. *J Neurosci* 22(17):7373–7379.

19. Cook A, et al. (2006) Caenorhabditis elegans ivermectin receptors regulate locomotor behaviour and are functional orthologues of Haemonchus contortus receptors. *Mol Biochem Parasitol* 147(1):118–125.
20. Brownlee DJ, Holden-Dye L, Walker RJ (1997) Actions of the anthelmintic ivermectin on the pharyngeal muscle of the parasitic nematode, Ascaris suum. *Parasitology* 115(Pt 5): 553–561.
21. Moreno Y, Nabhan JF, Solomon J, Mackenzie CD, Geary TG (2010) Ivermectin disrupts the function of the excretory-secretory apparatus in microfilariae of Brugia malayi. *Proc Natl Acad Sci USA* 107(46):20120–20125.
22. Daeffler KN, Lester HA, Dougherty DA (2014) Functional evaluation of key interactions evident in the structure of the eukaryotic Cys-loop receptor GluCl. *ACS Chem Biol* 9(10):2283–2290.
23. Hibbs RE, Gouaux E (2011) Principles of activation and permeation in an anion-selective Cys-loop receptor. *Nature* 474(7349):54–60.
24. Miller PS, Aricescu AR (2014) Crystal structure of a human GABAA receptor. *Nature* 512(7514):270–275.
25. Bocquet N, et al. (2009) X-ray structure of a pentameric ligand-gated ion channel in an apparently open conformation. *Nature* 457(7225):111–114.
26. Hilf RJ, Dutzler R (2009) Structure of a potentially open state of a proton-activated pentameric ligand-gated ion channel. *Nature* 457(7225):115–118.
27. Pan J, et al. (2012) Structure of the pentameric ligand-gated ion channel ELIC cocrystallized with its competitive antagonist acetylcholine. *Nat Commun* 3:714.
28. Gonzalez-Gutierrez G, et al. (2012) Mutations that stabilize the open state of the Erwinia chrisanthemi ligand-gated ion channel fail to change the conformation of the pore domain in crystals. *Proc Natl Acad Sci USA* 109(16):6331–6336.
29. Howard RJ, et al. (2011) Structural basis for alcohol modulation of a pentameric ligand-gated ion channel. *Proc Natl Acad Sci USA* 108(29):12149–12154.
30. Spurny R, et al. (2012) Pentameric ligand-gated ion channel ELIC is activated by GABA and modulated by benzodiazepines. *Proc Natl Acad Sci USA* 109(44):E3028–E3034.
31. Brejc K, et al. (2001) Crystal structure of an ACh-binding protein reveals the ligand-binding domain of nicotinic receptors. *Nature* 411(6835):269–276.
32. Celie PH, et al. (2004) Nicotine and carbamylcholine binding to nicotinic acetylcholine receptors as studied in AChBP crystal structures. *Neuron* 41(6):907–914.
33. Hansen SB, et al. (2005) Structures of Aplysia AChBP complexes with nicotinic agonists and antagonists reveal distinctive binding interfaces and conformations. *EMBO J* 24(20):3635–3646.
34. Hibbs RE, et al. (2009) Structural determinants for interaction of partial agonists with acetylcholine binding protein and neuronal alpha7 nicotinic acetylcholine receptor. *EMBO J* 28(19):3040–3051.
35. Grosman C, Salamone FN, Sine SM, Auerbach A (2000) The extracellular linker of muscle acetylcholine receptor channels is a gating control element. *J Gen Physiol* 116(3):327–340.
36. Kash TL, Jenkins A, Kelley JC, Trudell JR, Harrison NL (2003) Coupling of agonist binding to channel gating in the GABA(A) receptor. *Nature* 421(6920):272–275.
37. Bouzat C, et al. (2004) Coupling of agonist binding to channel gating in an ACh-binding protein linked to an ion channel. *Nature* 430(7002):896–900.
38. Reeves DC, Jansen M, Bali M, Lemster T, Akabas MH (2005) A role for the beta 1-beta 2 loop in the gating of 5-HT3 receptors. *J Neurosci* 25(41):9358–9366.
39. Jha A, Cadugan DJ, Purohit P, Auerbach A (2007) Acetylcholine receptor gating at extracellular transmembrane domain interface: the cys-loop and M2-M3 linker. *J Gen Physiol* 130(6):547–558.
40. Bouzat C, Bartos M, Corradi J, Sine SM (2008) The interface between extracellular and transmembrane domains of homomeric Cys-loop receptors governs open-channel lifetime and rate of desensitization. *J Neurosci* 28(31):7808–7819.
41. Lee WY, Free CR, Sine SM (2009) Binding to gating transduction in nicotinic receptors: Cys-loop energetically couples to pre-M1 and M2-M3 regions. *J Neurosci* 29(10):3189–3199.
42. Perkins DI, et al. (2009) Loop 2 structure in glycine and GABA(A) receptors plays a key role in determining ethanol sensitivity. *J Biol Chem* 284(40):27304–27314.
43. Pless SA, Lynch JW (2009) Magnitude of a conformational change in the glycine receptor beta1-beta2 loop is correlated with agonist efficacy. *J Biol Chem* 284(40): 27370–27376.
44. Wiltfong RE, Jansen M (2009) Probing protein packing surrounding the residues in and flanking the nicotinic acetylcholine receptor M2M3 loop. *J Neurosci* 29(6): 1626–1635.
45. Frazier SJ, Cohen BN, Lester HA (2013) An engineered glutamate-gated chloride (GluCl) channel for sensitive, consistent neuronal silencing by ivermectin. *J Biol Chem* 288(29):21029–21042.
46. Yoluk O, Brömstrup T, Bertaccini EJ, Trudell JR, Lindahl E (2013) Stabilization of the GluCl ligand-gated ion channel in the presence and absence of ivermectin. *Biophys J* 105(3):640–647.
47. Monod J, Wyman J, Changeux JP (1965) On the nature of allosteric transitions: A plausible model. *J Mol Biol* 12:88–118.
48. Karlin A (1967) On the application of "a plausible model" of allosteric proteins to the receptor for acetylcholine. *J Theor Biol* 16(2):306–320.
49. Edelstein SJ, Changeux JP (1996) Allosteric proteins after thirty years: The binding and state functions of the neuronal alpha 7 nicotinic acetylcholine receptors. *Experientia* 52(12):1083–1090.
50. Auerbach A (2012) Thinking in cycles: MWC is a good model for acetylcholine receptor-channels. *J Physiol* 590(Pt 1):93–98.
51. Corringer PJ, et al. (1999) Mutational analysis of the charge selectivity filter of the alpha7 nicotinic acetylcholine receptor. *Neuron* 22(4):831–843.
52. Pittel I, Witt-Kehati D, Degani-Katzav N, Paas Y (2010) Probing pore constriction in a ligand-gated ion channel by trapping a metal ion in the pore upon agonist dissociation. *J Biol Chem* 285(34):26519–26531.
53. Chang Y, Weiss DS (1999) Allosteric activation mechanism of the alpha 1 beta 2 gamma 2 gamma-aminobutyric acid type A receptor revealed by mutation of the conserved M2 leucine. *Biophys J* 77(5):2542–2551.
54. Forman SA (2012) Monod-Wyman-Changeux allosteric mechanisms of action and the pharmacology of etomidate. *Curr Opin Anaesthesiol* 25(4):411–418.
55. Etter A, et al. (1999) Picrotoxin blockade of invertebrate glutamate-gated chloride channels: Subunit dependence and evidence for binding within the pore. *J Neurochem* 72(1):318–326.
56. Burnham KP, Anderson DR (2002) *Model Selection and Multimodel Inference: A Practical Information-Theoretic Approach* (Springer, New York), 2nd Ed.
57. Wagoner KR, Czajkowski C (2010) Stoichiometry of expressed alpha(4)beta(2)delta gamma-aminobutyric acid type A receptors depends on the ratio of subunit cDNA transfected. *J Biol Chem* 285(19):14187–14194.
58. Krashia P, et al. (2010) Human $\alpha3\beta4$ neuronal nicotinic receptors show different stoichiometry if they are expressed in Xenopus oocytes or mammalian HEK293 cells. *PLoS One* 5(10):e13611.
59. Harpsøe K, et al. (2011) Unraveling the high- and low-sensitivity agonist responses of nicotinic acetylcholine receptors. *J Neurosci* 31(30):10759–10766.
60. Mazzaferro S, et al. (2011) Additional acetylcholine (ACh) binding site at alpha4/alpha4 interface of (alpha4beta2)2alpha4 nicotinic receptor influences agonist sensitivity. *J Biol Chem* 286(35):31043–31054.
61. Ahring PK, et al. (2015) Engineered $\alpha4\beta2$ nicotinic acetylcholine receptors as models for measuring agonist binding and effect at the orthosteric low-affinity $\alpha4$-$\alpha4$ interface. *Neuropharmacology* 92:135–145.
62. Sancar F, Czajkowski C (2011) Allosteric modulators induce distinct movements at the GABA-binding site interface of the GABA-A receptor. *Neuropharmacology* 60(2-3): 520–528.
63. Hanson SM, Czajkowski C (2008) Structural mechanisms underlying benzodiazepine modulation of the GABA(A) receptor. *J Neurosci* 28(13):3490–3499.
64. Wang DS, Mangin JM, Moonen G, Rigo JM, Legendre P (2006) Mechanisms for picrotoxin block of alpha2 homomeric glycine receptors. *J Biol Chem* 281(7):3841–3855.
65. Nelson ME, Kuryatov A, Choi CH, Zhou Y, Lindstrom J (2003) Alternate stoichiometries of alpha4beta2 nicotinic acetylcholine receptors. *Mol Pharmacol* 63(2):332–341.
66. Plazas PV, Katz E, Gomez-Casati ME, Bouzat C, Elgoyhen AB (2005) Stoichiometry of the alpha9alpha10 nicotinic cholinergic receptor. *J Neurosci* 25(47):10905–10912.
67. Moroni M, Zwart R, Sher E, Cassels BK, Bermudez I (2006) alpha4beta2 nicotinic receptors with high and low acetylcholine sensitivity: pharmacology, stoichiometry, and sensitivity to long-term exposure to nicotine. *Mol Pharmacol* 70(2):755–768.
68. Gu Y, Camacho P, Gardner P, Hall ZW (1991) Identification of two amino acid residues in the epsilon subunit that promote mammalian muscle acetylcholine receptor assembly in COS cells. *Neuron* 6(6):879–887.
69. Kreienkamp HJ, Maeda RK, Sine SM, Taylor P (1995) Intersubunit contacts governing assembly of the mammalian nicotinic acetylcholine receptor. *Neuron* 14(3):635–644.
70. Green WN, Wanamaker CP (1997) The role of the cystine loop in acetylcholine receptor assembly. *J Biol Chem* 272(33):20945–20953.
71. Bar-Lev DD, Degani-Katzav N, Perelman A, Paas Y (2011) Molecular dissection of Cl–selective Cys-loop receptor points to components that are dispensable or essential for channel activity. *J Biol Chem* 286(51):43830–43841.
72. Adams DJ, Gage PW (1979) Characteristics of sodium and calcium conductance changes produced by membrane depolarization in an Aplysia neurone. *J Physiol* 289: 143–161.
73. Fenwick EM, Marty A, Neher E (1982) Sodium and calcium channels in bovine chromaffin cells. *J Physiol* 331:599–635.
74. Hosoya Y, Yamada M, Ito H, Kurachi Y (1996) A functional model for G protein activation of the muscarinic K+ channel in guinea pig atrial myocytes. Spectral analysis of the effect of GTP on single-channel kinetics. *J Gen Physiol* 108(6):485–495.
75. Wang F, Zeltwanger S, Yang IC, Nairn AC, Hwang TC (1998) Actions of genistein on cystic fibrosis transmembrane conductance regulator channel gating. Evidence for two binding sites with opposite effects. *J Gen Physiol* 111(3):477–490.
76. Collier ML, Hume JR (1995) Unitary chloride channels activated by protein kinase C in guinea pig ventricular myocytes. *Circ Res* 76(2):317–324.
77. Kiefer F, Arnold K, Künzli M, Bordoli L, Schwede T (2009) The SWISS-MODEL Repository and associated resources. *Nucleic Acids Res* 37(Database issue):D387–D392.